

# On the Clustering of Faint Red Galaxies

Haojie Xu<sup>1\*</sup>, Zheng Zheng<sup>1</sup>, Hong Guo<sup>2,1</sup>, Ju Zhu<sup>3</sup>, and Idit Zehavi<sup>4</sup>

<sup>1</sup> Department of Physics and Astronomy, University of Utah, 115 South 1400 East, Salt Lake City, UT 84112, USA

<sup>2</sup> Shanghai Astronomical Observatory, Chinese Academy of Sciences, Shanghai 200030, China

<sup>3</sup> Department of Astronomy, University of Illinois at Urbana-Champaign, MC-221, 1002 W. Green Street, Urbana, IL 61801, USA

<sup>4</sup> Department of Astronomy, Case Western Reserve University, 10900 Euclid Avenue, Cleveland, OH 44106, USA

June 6, 2016

## ABSTRACT

Faint red galaxies in the Sloan Digital Sky Survey show a puzzling clustering pattern in previous measurements. In the two-point correlation function (2PCF), they appear to be strongly clustered on small-scales, indicating a tendency to reside in massive haloes as satellite galaxies. However, their weak clustering on large scales suggests that they are more likely to be found in low mass haloes. The interpretation of the clustering pattern suffers from the large sample variance in the 2PCF measurements, given the small volume of the volume-limited sample of such faint galaxies. We present improved clustering measurements of faint galaxies by making a full use of a flux-limited sample to obtain volume-limited measurements with an increased effective volume. In the improved 2PCF measurements, the fractional uncertainties on large-scales drop by more than 40 per cent, and the strong contrast between small-scale and large-scale clustering amplitudes seen in previous work is no longer prominent. From halo occupation distribution modelling of the measurements, we find that a considerable fraction of faint red galaxies to be satellites in massive haloes, a senario supported by the strong covariance of small-scale 2PCF measurements and the relative spatial distribution of faint red galaxies and luminous galaxies. However, the satellite fraction is found to be degenerate with the slope of the distribution profile of satellites in inner haloes. We compare the modelling results with semi-analytic model predictions and discuss the implications.

**Key words:** cosmology: observations – cosmology: theory – galaxies: clusters: general – galaxies: distances and redshifts – galaxies: haloes – galaxies: statistics – large-scale structure of Universe

## 1 INTRODUCTION

Galaxy clustering measured in large galaxy redshift surveys encodes important information about galaxy formation and evolution. In particular, galaxy clustering measurements, in combination with the theoretically well-understood dark matter halo population for a given cosmology, enable the inference of the relation between galaxies and dark matter haloes, with halo-based clustering model (e.g. Jing, Mo & Borner 1998; Peacock & Smith 2000; Seljak 2000; Scoccimarro et al. 2001; Berlind & Weinberg 2002; Yang et al. 2003; Zheng et al. 2005). In this work, we focus on measuring and modeling the clustering of a population of faint red galaxies and discuss the corresponding implications on their formation and evolution.

Galaxies occupying the faint, red corner of the galaxy colour-magnitude diagram display interesting properties. Using Sloan Digital Sky Survey (SDSS; York et al. 2000) data, Hogg et al. (2003) and Blanton et al. (2005a) find that both the faint and bright

red galaxies have the highest galaxy over-densities within spheres of radii  $1h^{-1}\text{Mpc}$  and  $8h^{-1}\text{Mpc}$ , indicating the high density environments they reside in. Norberg et al. (2002) analyse the 2dF Galaxy Redshift Survey data and concludes that the faint, early-type galaxies has nearly the same clustering strength with bright ones, which contrasts the idea that brighter galaxies usually have stronger clustering strength. With the early SDSS data, Zehavi et al. (2005; hereafter Z05) find that the two-point correlation function (2PCF) of faint red galaxies rises steeply toward small scales ( $\lesssim 2h^{-1}\text{Mpc}$ ). In particular, the feature is prominent in the faintest sample ( $-19 < M_r < -18$ ) they analysed. In addition, the 2PCF of this sample shows a quite low clustering amplitude on large scales ( $\gtrsim 2h^{-1}\text{Mpc}$ ). These features are not seen in the blue galaxies. The result is further confirmed with the analysis of the data from the completed SDSS survey (Zehavi et al. 2011; hereafter Z11) — the small-scale clustering amplitude is as high as that of the brightest sample ( $\sim 4$  magnitudes more luminous), in strong contrast to the low large-scale clustering amplitude. The case is even more extreme for a fainter sample with  $-18 < M_r < -17$  (whose 2PCF measurements have a low signal-to-noise ratio though).

\* E-mail: haojie.xu@utah.edu

The strong non-linearity in the 2PCF towards small scales, together with the small-scale redshift-space distortion, can explain the scale- and method-dependent galaxy bias factor determined for the faint red galaxies from many previous studies (e.g. Li et al. 2006a; Swanson et al. 2008; Cresswell & Percival 2009; Zehavi et al. 2011), as investigated in detail by Ross et al. (2011).

The strong small-scale clustering indicates that the faint red galaxies tend to reside in massive haloes, while the weak large-scale clustering suggests that they are more likely to be found in low mass haloes. This puzzling result leads to some difficulty in modeling the 2PCF within the HOD framework. The simple HOD model in Z11 results in a satellite fraction of 90 per cent, with a poor fit. The other model Z11 considered is that the  $-19 < M_r < -18$  faint red galaxies are composed of central galaxies in haloes of a few times  $10^{11} h^{-1} M_\odot$  and satellite galaxies in haloes more massive than  $10^{13} h^{-1} M_\odot$ , with no galaxies in host haloes of mass in between. The model leads to a satellite fraction of 34 per cent, but it still cannot provide a good explanation of the low amplitude at large scales. Other statistics are also used to study faint red galaxies. The red galaxy pairwise velocity dispersion on small scales peak around  $M_r = -19.5$  (Li et al. 2006b), which supports the scenario that a fraction of the faint red galaxies are satellites in massive haloes. With a group catalog, Wang et al. (2009) study red galaxies with much lower luminosity and infer that about 55–65 per cent of  $M_r \sim -17$  red galaxies are satellites.

Different processes may be at work to quench star formation in central and satellite galaxies, causing them to turn red. If the faint red galaxies are central galaxies in low mass haloes ( $\sim 10^{11} h^{-1} M_\odot$ ), star formation feedback can be responsible for shutting down the star formation. If the faint red galaxies are satellites in massive haloes, environmental effects (e.g. strangulation, ram pressure stripping, and tidal heating and stripping) are the more likely causes. A better determination of the central and satellite status of the faint red galaxies can help to constrain their formation. Using galaxy clustering for such a study relies on accurate clustering measurements. However, given the low luminosity of the faint red galaxies, they cannot be observed to large distances in a flux-limited galaxy redshift survey, like the SDSS. The clustering measurements, which are usually done with volume-limited samples, suffer from substantial sample variance with the small survey volume for faint galaxies. One way to overcome the limitation is to study the angular clustering with the (deeper) photometric sample (e.g. Ross et al. 2011). In this paper, we focus on a maximal use of the spectroscopic sample to improve the clustering measurements of faint galaxies and investigate what constraints we can put on their nature through HOD modeling.

In Section 2, we describe the data and clustering measurements. In Section 3, we present the method to measure the 2PCF in a volume-limited sense with the full use of a flux-limited sample, improving the measurements by effectively increasing the volume. A detailed derivation of the method is given in Appendix A. The results from HOD modeling of the improved 2PCF is presented in Section 4. Finally, we summarize and discuss the results in Section 5.

## 2 OBSERVATIONS AND METHODS

### 2.1 Data

We study the faint red galaxies in the MAIN sample (Strauss et al. 2002) of the SDSS (York et al. 2000; Stoughton et al. 2002). The

data we use are from the SDSS Data Release 7 (hereafter SDSS DR7; Abazajian et al. 2009), which is the end data release of SDSS-II. We take the large-scale structure sample in the NYU Value-Added Galaxy Catalog<sup>1</sup> (NYU-VAGC; Blanton et al. 2005b; Adelman-McCarthy et al. 2008; Padmanabhan et al. 2008), which covers a sky area of 7,966 deg<sup>2</sup>. We adopt the full flux-limited sample, and in Section 3, we show how to use the sample in a pairwise volume-limited sense. The magnitude in the sample has been  $K$ -corrected and we further apply an evolution correction to  $z \sim 0.1$  (Z11). Galaxies with  $-19 < M_r < -18$  are selected from the NYU-VAGC bright sample with  $r < 17.6$ . Finally we define our faint red galaxy sample by imposing the colour selection  $g - r > 0.21 - 0.03 M_r$ , as in Z11. In total, we end up with 11,357 faint red galaxies.

For the clustering measurements, we also use the corresponding random catalogs provided by the NYU-VAGC, which takes accounted for the complex survey geometry and detailed angular selection function. Compared to the galaxy catalog, the random catalog we use contains 50 times as many galaxies.

Throughout the paper, all distances and galaxy pair separations are expressed in comoving units. For all distance calculations, we assume a flat  $\Lambda$ CDM cosmological model with  $\Omega_m = 0.25$ . Since the sample is at  $z \sim 0$ , the results are not sensitive to this choice of  $\Omega_m$ . The Hubble constant is taken to be  $H_0 = 100 h \text{ km s}^{-1} \text{ Mpc}^{-1}$  with  $h = 0.7$ , while the absolute magnitudes of galaxies are expressed by adopting  $h = 1$ .

### 2.2 Methods

We characterize the clustering of galaxies with the 2PCF, the excess probability of finding galaxy pairs at a given separation with respect to a random distribution (Peebles 1980). For a pair of galaxies with redshift positions  $\mathbf{v}_1$  and  $\mathbf{v}_2$ , we compute the separation ( $\pi$ ) parallel to the line of sight and that ( $r_p$ ) perpendicular to the line of sight as

$$\pi \equiv |\mathbf{s} \cdot \mathbf{l}|/|\mathbf{l}|, \quad r_p^2 \equiv \mathbf{s} \cdot \mathbf{s} - \pi^2, \quad (1)$$

where  $\mathbf{s} \equiv \mathbf{v}_1 - \mathbf{v}_2$  is the redshift separation vector and  $\mathbf{l} \equiv (\mathbf{v}_1 + \mathbf{v}_2)/2$  is the line-of-sight vector (Fisher et al. 1994).

The widely adopted estimator to calculate the redshift-space galaxy 2PCF  $\xi(r_p, \pi)$  is given by Landy & Szalay (1993),

$$\xi(r_p, \pi) = \frac{\text{DD} - 2\text{DR} + \text{RR}}{\text{RR}}, \quad (2)$$

where DD, DR, and RR are the numbers of data-data, data-random and random-random pairs in each separation bin, normalized by the corresponding total pair counts  $N_D(N_D - 1)/2$ ,  $N_D N_R$  and  $N_R(N_R - 1)/2$  (with  $N_D$  and  $N_R$  the total numbers of galaxies and random points), respectively. In Section 3, we propose to measure the 2PCF using the flux-limited sample but with appropriate volume weight for each galaxy pair to reach an effectively volume-limited measurement. The method can make full use of the observation and measure the 2PCF more accurately. The generalized estimator is presented in Appendix A and discussed in Section 3.

From the measured  $\xi(r_p, \pi)$ , we compute the projected 2PCF

$$w_p(r_p) = 2 \int_0^\infty d\pi \xi(r_p, \pi), \quad (3)$$

which intends to remove the redshift-space distortion effect. For

<sup>1</sup> <http://sdss.physics.nyu.edu/lss.html>

the faint red galaxy sample studied in this paper, we integrate up to  $\pi_{\max} = 40h^{-1}\text{Mpc}$ , which is also adopted consistently in the HOD modeling of the clustering result. In our measurements, we use linearly spaced bins in  $\pi$  with widths of  $1h^{-1}\text{Mpc}$  and logarithmically spaced  $r_p$  bins with 0.2 dex width.

Finally, to estimate the covariance matrix of the measured  $w_p$ , we apply the jackknife resampling method (e.g., Z05, Z11) with  $N = 146$  spatially contiguous subsamples of the full data set with equal area. We measure the projected 2PCF  $w_p^l$  for the  $l$ -th jackknife sample ( $l = 1, 2, \dots, N$ ), which omits the  $l$ -th subsample, and the covariance matrix is then estimated as

$$\text{Covar}(w_{p,i}, w_{p,j}) = \frac{N-1}{N} \sum_{l=1}^N (w_{p,i}^l - \bar{w}_{p,i})(w_{p,j}^l - \bar{w}_{p,j}), \quad (4)$$

where  $w_{p,i}^l$  is the value of  $w_p$  at the  $i$ -th projected pair separation bin  $r_{p,i}$  measured from the  $l$ -th jackknife sample, and  $\bar{w}_{p,i}$  is the value of  $w_p$  in such a bin averaged over all jackknife samples.

### 3 PAIRWISE VOLUME-LIMITED 2PCF MEASUREMENTS FROM THE FLUX-LIMITED SAMPLE

In large galaxy redshift surveys, volume-limited galaxy samples are preferred for galaxy clustering study (e.g., Z05, Z11), since the samples are well-defined within the volume to have uniform properties (e.g., the same range of luminosities across the volume). The measured 2PCFs from volume-limited samples also make it easy to interpret with theoretical models. For example, with HOD modeling of the clustering of volume-limited samples, we can infer meaningful information about the relation between galaxy properties (e.g., luminosity) and halo mass.

However, the natural product from a galaxy redshift survey is a flux-limited galaxy sample, which is substantially larger than any volume-limited sample constructed for galaxy clustering study. The volume (or maximum redshift) for a volume-limited sample is determined by requiring that all type of galaxies in the sample to be complete within the volume. For some galaxies, even though their properties can make them fall into the sample of interest, they are excluded because they fall outside of the volume of completeness. This greatly limits the statistical power of the volume-limited sample. To have better statistics for the clustering of galaxies, it is desirable to include as many galaxies as possible while still keeping the volume-limited nature of the 2PCF measurements. This is particularly important for faint galaxies, given the expected small volume for constructing a full volume-limited sample. We propose here a method of measuring galaxy 2PCFs by making full use of galaxies in a flux-limited sample and giving each pair of galaxies an appropriate weight, which will lead to effectively volume-limited 2PCF measurements. The method is termed as pairwise volume-limited 2PCF measurements, whose meaning will become clear later.

We use the faint red galaxy sample to illustrate the basic idea of the method and present the final pairwise volume-limited 2PCF measurements to be used for the HOD modeling.

In the left panel of Figure 1, we show the construction of the volume-limited sample for  $-19 < M_r < -18$  red galaxies, as used in previous studies (e.g., Z11). The points denote a random selection of the red galaxies within the  $-19 < M_r < -18$  magnitude bin that are observed in the SDSS-II DR7, which are flux limited. The right boundary of the points reflects the flux limit or the faint magnitude limit  $r = 17.6$ . To construct the volume-limited sample, both the galaxies at the faint end ( $M_r = -18$ ) and at the

bright end ( $M_r = -19$ ) need to be complete, and the maximum redshift is then completely determined by the faintest galaxies in the sample of interest (i.e.  $M_r = -18$ ). As a consequence, only galaxies within the red box enter the volume-limited sample. The maximum redshift is  $z_{\max} = 0.042$ . In principle, the minimum redshift can go to zero, but here we follow Z11 to fix it at  $z_{\min} = 0.017$  to avoid low  $z$  incompleteness, which only reduces the volume by  $\sim 7$  per cent. The volume-limited sample constructed this way is composed of 5,165 galaxies. It clearly excludes all the galaxies beyond  $z_{\max}$ , because they are not complete in the full range of the above magnitude bin. The number of such galaxies is not small,  $\sim 6,000$ , comparable to that in the volume-limited sample. If they can be used for measuring the 2PCFs, we would achieve a better statistic.

The middle panel of Figure 1 shows a case on how to make use of the galaxies beyond  $z_{\max}$ , which can be treated as an instructive example and an intermediate step towards the method we propose. We divide the  $-18 < M_r < -19$  red galaxies into two subsamples — the faint and bright subsamples are made of galaxies with  $-18 < M_r < -18.5$  and  $-18.5 < M_r < -19$ , respectively. The principle underlying our method is that galaxy pairs are made of faint-faint pairs, faint-bright pairs, and bright-bright pairs. In terms of the 2PCF  $\xi$ , it can be decomposed into contributions from the auto-correlation  $\xi_{ff}$  of galaxies in the faint subsample, the cross-correlation  $\xi_{fb}$  between galaxies in the faint and bright subsamples, and the auto-correlation  $\xi_{bb}$  of galaxies in the bright subsamples. The total 2PCF can be expressed as (Zu et al. 2008)

$$\xi = \frac{\bar{n}_f^2}{\bar{n}^2} \xi_{ff} + \frac{2\bar{n}_b\bar{n}_f}{\bar{n}^2} \xi_{fb} + \frac{\bar{n}_b^2}{\bar{n}^2} \xi_{bb}, \quad (5)$$

where  $\bar{n}_f$ ,  $\bar{n}_b$ , and  $\bar{n}$  are the galaxy number densities in the faint subsample, the bright subsample, and the full sample, respectively.

The auto-correlation  $\xi_{ff}$  of galaxies in the faint subsample can be measured with the volume-limited faint subsample, whose volume is illustrated by the bottom red rectangle box in the middle panel of Figure 1. It has the same  $z_{\max}$  as the case in the left panel. For the cross-correlation  $\xi_{fb}$  between the faint and bright subsamples, the volume-limited measurements are also made in the above volume, i.e., the same as in the left panel. However, for the auto-correlation  $\xi_{bb}$  of galaxies in the bright subsample, we are able to perform the measurement in a much larger volume, as illustrated by the top (solid) red rectangle in the middle panel. It reaches up to  $z_{\max} = 0.053$ , and the galaxies in the bright sample are complete in this volume. That is, we are able to measure  $\xi_{bb}$  in a volume almost twice larger than in the previous case, which reduces the uncertainty (sample variance) in  $\xi_{bb}$  and hence improves the measurement in the total  $\xi$  [equation (5)]. The measurement is still a volume-limited one — we do not change the component contributions to the total  $\xi$ , but just make the measurement more accurate for the bright-bright auto-correlation contribution. In other words, we increase the effective volume for the 2PCF measurement.

Figure 2 shows the measurements of different component 2PCFs and compare the results corresponding to the case in the middle panel with the usual volume-limited case in the left panel of Figure 1. For simplicity, below we use  $\xi$  to denote the clustering measurements of interest here, i.e.,  $w_p$ . The components  $\xi_{ff}$  (red curve) and  $\xi_{fb}$  (green curve) are the same for the two cases. The component  $\xi_{bb}$  shows a clear difference. The  $\xi_{bb}$  measured in the larger volume (solid blue curve) is higher in amplitude, compared to that measured in the smaller volume (dashed blue curve). This is clearly a sample variance effect, and the one measured in the larger volume is less affected. The fractional uncertainties (middle panel)

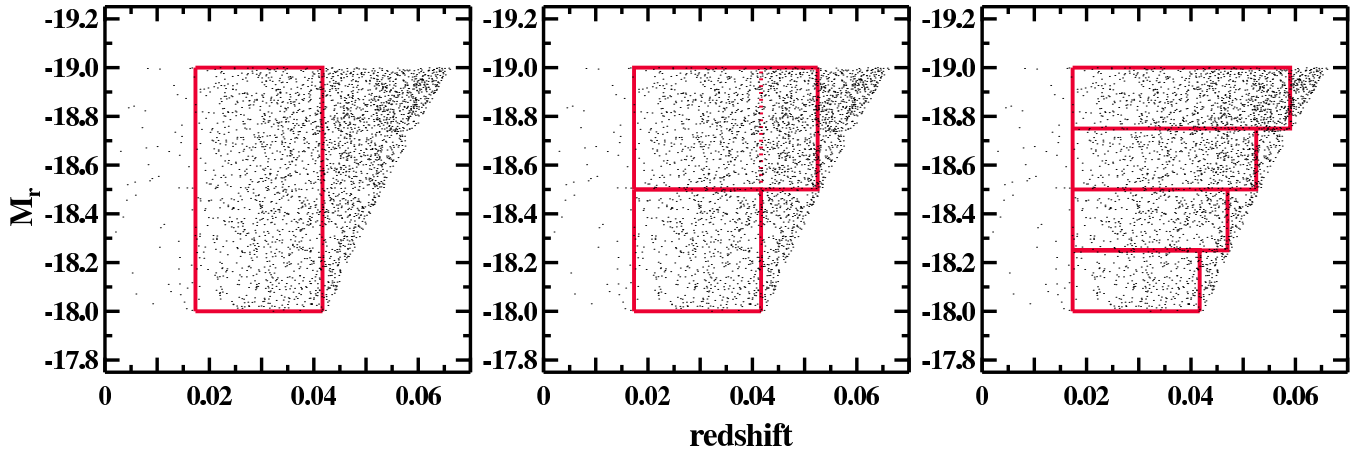


**Figure 1.** Illustration of different ways of sample construction in measuring the 2PCF of red galaxies in the luminosity bin of  $-19 < M_r < -18$  in a volume-limited sense. In each panels, the minimum redshift  $z_{\min} = 0.017$ , delineating by the left vertical line. The dots show a random selection of the flux-limited sample, with the right boundary set by the flux limit. *Left:* The commonly adopted volume-limited sample, with the maximum redshift (the right side of the red rectangle) determined by the faint boundary of the luminosity bin. *Middle:* Galaxies are divided into two subsamples. The contribution to the 2PCF from the bright galaxies can be measured within the larger volume (top rectangle), reducing the effect of sample variance. *Right:* Galaxies are divided into four subsamples, with different volumes. More galaxies and an effectively larger volume are used in measuring the 2PCF. The method introduced in this work can be thought as dividing galaxies into subsamples of infinitesimally small luminosity bins, achieving a maximal use of the flux-limited data for an effectively volume-limited 2PCF measurement. See the text for details.

estimated from the jackknife method also shows that the larger volume reduces the uncertainties in the measurements. Because of the improvement in the  $\xi_{bb}$  measurements, the uncertainties in the total  $\xi$  are reduced by 20-40 per cent, especially on large scales (bottom panel). By comparing the solid and dashed black curves, we find that the improved  $\xi$  measurement no longer shows the steep drop at  $r_p > 2h^{-1}\text{Mpc}$  seen in Z11.

We see that dividing the sample into faint and bright subsamples enables us to improve the 2PCF measurements. However, we still exclude many galaxies, i.e. galaxies at redshifts higher than those set by the volume-limited faint and bright subsamples. These are the points out of the right boundaries of the top and bottom solid rectangles in the middle panel of Figure 1.

To incorporate more galaxies into the measurements, we can make further division for the faint and bright subsamples. That is, we divide the whole sample into more subsamples with finer luminosity bins. Following Zu et al. (2008), equation (5) is then generalized to

$$\xi = \sum_{i,j} \frac{\bar{n}_i \bar{n}_j}{\bar{n}^2} \xi_{ij}, \quad (6)$$

where  $\bar{n}_i$  is the mean number density of the  $i$ -th subsample and  $\xi_{ij}$  is the 2-point cross-correlation function between galaxies in the  $i$ -th and  $j$ -th subsample (autocorrelation function if  $i = j$ ). Both  $i$  and  $j$  go from 1 to  $N$ , the number of luminosity bins. We can construct volume-limited sample for each subsample. Given the difference in luminosity, different subsamples have different values of  $z_{\max}$  or volumes of completeness. Except for the faintest sample, the volumes are all larger than the one used in the left panel of Figure 1. When measuring  $\xi_{ij}$ , we just need to use galaxies in the volume defined by the fainter one of the  $i$ -th and  $j$ -th subsamples. The right panel of Figure 1 illustrates one case of dividing the sample into four subsamples, and we can see that the volume to be used increases with the luminosity of the subsample. Compared to the middle panel, more galaxies are included in the 2PCF measurements, and we expect the measurements to be further improved, reducing the effect of sample variance.

In Appendix A, we prove that the 2PCF with such a division can be calculated with the following generalized Landy-Szalay estimator,

$$\xi = \frac{\sum_{i,j} \frac{1}{V_{ij}} \text{DD}_{ij}|_{V_{ij}} - 2 \sum_{i,j} \frac{1}{V_{ij}} \text{DR}_{ij}|_{V_{ij}} + \sum_{i,j} \frac{1}{V_{ij}} \text{RR}_{ij}|_{V_{ij}}}{\sum_{i,j} \frac{1}{V_{ij}} \text{RR}_{ij}|_{V_{ij}}}. \quad (7)$$

Here  $V_{ij} = \min\{V_i, V_j\}$ , where  $V_i$  and  $V_j$  are the volumes of completeness corresponding to the  $i$ -th and  $j$ -th luminosity bin given the flux limit. The quantity  $\text{DD}_{ij}|_{V_{ij}}$  is the normalized number of galaxy pairs within  $V_{ij}$ , with each pair composed of one galaxy in the  $i$ -th luminosity bin and one in the  $j$ -th luminosity bin, and similarly for  $\text{DR}_{ij}|_{V_{ij}}$  and  $\text{RR}_{ij}|_{V_{ij}}$ . Note that for our purpose here, each point in the random catalog is assigned with a luminosity so that the luminosity and redshift distributions of the galaxy sample are reproduced. The way we construct the random catalog is as follows. For each random point, we take the angular position in the original random catalog and assign a luminosity randomly chosen from the galaxy catalog. We then assign a redshift to this random point in the range of  $(z_{\min}, z_{\max})$ , where  $z_{\min} = 0.017$  and  $z_{\max}$  is determined from the luminosity and the flux limit. The redshift is assigned such that galaxies are uniformly distributed in the comoving volume set by  $z_{\min}$  and  $z_{\max}$  (i.e.  $D_c^3$ , the cube of the comoving distance, follows a uniform distribution).

Conceptually, the ultimate limit of the division is that there is one galaxy per fine luminosity bin, which has a corresponding maximum volume determined from the luminosity and the flux limit. This is the limit that we apply equation (7) to compute the 2PCF. In detail, for each galaxy-galaxy, galaxy-random, or random-random pair, we check whether both galaxies fall into the volume  $V_{ij}$  (which is determined by the fainter galaxy of the pair). If they do, we keep the pair and weigh it by  $1/V_{ij}$ . The generalized estimator in equation (7) can reduce to the same form as the Landy-Szalay estimator [equation (2)], with the DD, DR, and RR terms being understood as the total count of pairs that pass the above criterion with each weighted by  $1/V_{ij}$ . We note that Li et al. (2006a), Li & White



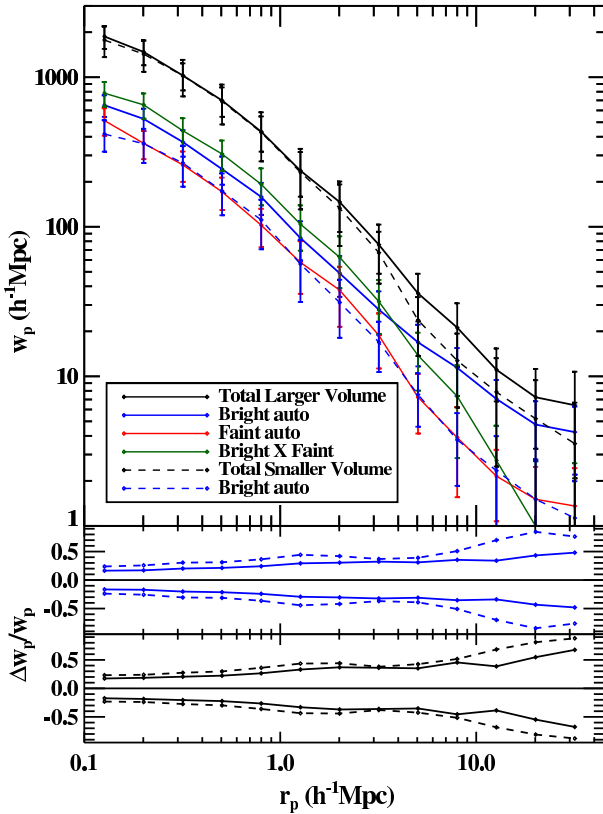


**Figure 2.** Decomposition of the projected 2PCF of the  $-19 < M_r < -18$  red galaxies with the sample division illustrated in the middle panel of Figure 1. With the sample divided into the faint and bright subsamples, the total 2PCF (solid black) is contributed by the faint-faint auto-correlation (solid red), the faint-bright cross-correlation (solid green), and the bright-bright auto-correlation (solid blue). The first two are measured in a smaller volume with  $z_{\max} = 0.042$ , while the last one in a larger volume with  $z_{\max} = 0.053$  (Fig. 1). For comparison, the total and the bright-bright 2PCF measured in the smaller volume are also shown (dashed black and blue), corresponding to the case with the commonly adopted volume-limited sample illustrated in the left panel of Figure 1. The middle and bottom panels compare the fractional uncertainties in the bright-bright and total 2PCFs, respectively.

(2009) and Li et al. (2012) apply a similar  $1/V$  weight (explicitly mentioned but without a derivation; with  $V$  the smaller  $V_{\max}$  of the two galaxies) to galaxy pairs in estimating the distribution of stellar mass in the universe and the stellar-mass-dependent galaxy clustering. See Appendix A for a discussion of the subtle difference between our method and theirs.

Since we count each pair in a volume-limited sense, we call the measurements from this method as pairwise volume-limited measurements. Clearly this method makes the maximal use of the data, trying to account for contributions from every possible galaxy pair that belong to the sample. The measurements are still effectively volume-limited, since the component 2PCF is computed within the respective volume that ensures the completeness of the subsamples of interest. Compared to the original, commonly used volume-limited sample, which we denote it as ‘faint-end volume-limited’, the new method measures the 2PCF contributions from brighter galaxies in the sample in a larger volume. This helps to reduce the sample variance effect, and improve the overall 2PCF measurements. One may wonder whether the different volumes used to compute the component 2PCFs complicate the estimation

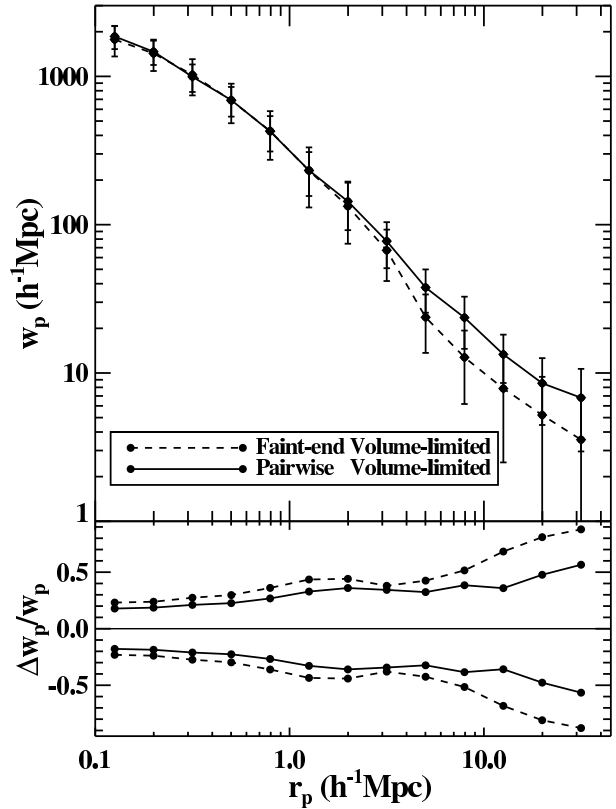


**Figure 3.** Projected 2PCF measurements (top) and fractional uncertainties (bottom) of the  $-19 < M_r < -18$  red galaxies from two methods. The dashed curves correspond to the case with the commonly adopted volume-limited sample (termed as ‘faint-end volume-limited’ here), and the solid curves are for the case of the pairwise volume-limited measurements with the flux-limited sample. See text for details.

of the covariance matrix. In fact, the covariance matrix is estimated using the jackknife method, and for each jackknife sample we apply the same generalized estimator. Therefore the variations in the volumes of different subsamples are automatically accounted for in the covariance matrix estimation. Not surprisingly, the method shares some similarities with the  $1/V_{\max}$  method used in estimating the luminosity function from a flux-limited galaxy survey — the  $1/V$  weight is used to estimate the number density of galaxies in deriving the luminosity function, (e.g. Schmidt 1968; Huchra & Sargent 1973), while it is used to effectively estimate the number density of galaxy pairs in our method.

We emphasize that the pairwise volume-limited measurement is different from the flux-limited measurement, even though both are based on the flux-limited galaxy sample. The flux-limited measurement does not remove any galaxy pairs and there is no weight given to each pair. In terms of the random sample, no luminosity information is needed, and we only need to ensure that the random points reproduce the angular and redshift distributions of the galaxy sample. Since brighter galaxies are observed to larger redshifts, they contribute more pairs than in a faint-end volume-limited case. As a consequence, the flux-limited 2PCF measurement effectively gives larger weights to the component 2PCF contributions from brighter galaxies, making it hard to interpret (see, however, Zu & Mandelbaum 2015, who manage to model the flux-limit measurements to gain an improved statistical power).

Finally, we apply the pairwise volume-limited method to the

faint red galaxy sample and compute the 2PCF to be used in the next section for HOD modeling. In the top panel of Figure 3, the solid curve shows the pairwise volume-limited  $w_p$  measurements. For comparison, the faint-end volume-limited measurements are plotted as the dashed curve, which are essentially the same as those obtained by Z11. Similar to the case in Figure 2, the full pairwise volume-limited measurements show enhanced clustering amplitudes on large scales, by a factor of about 60 per cent. The original finding by Z11 of a steep drop beyond  $r_p > 2h^{-1}\text{Mpc}$  is less prominent. The bottom panel shows the fractional uncertainties of the measurements. Those associated with the pairwise volume-limited measurements are smaller. Especially on large scales, the fractional uncertainties decrease by more than 40 per cent, which corresponds to an effective change in survey volume by a factor of two. We also applied this method to an even fainter sample, the red galaxies with  $-18 < M_r < -17$ , but the measurement is still noisy (like in Z11) because of the very limited sample size and volume.

The left panel of Figure 4 shows the covariance matrix estimated from the jackknife samples. It shows the interesting pattern that data points below  $3h^{-1}\text{Mpc}$  are highly correlated. This is in direct contrast to the pattern seen in the covariance matrices for bright galaxy samples. As a comparison, the right panel shows that for the  $M_r < -21$  sample, where the positive correlation occurs for data points on scales above  $3h^{-1}\text{Mpc}$ . A similar behavior was also found in Z05. We verified that the pattern seen in the covariance matrix for the  $M_r < -21$  sample remains similar, even if it is evaluated within a small volume. Therefore, the contrast in the covariance matrices for faint and bright galaxy samples is not caused by the difference in survey volume. It may reflect the difference in the way that galaxies occupy dark matter haloes and in the contribution from satellite galaxies, which will be discussed further in the Section 4.

Before switching to the HOD modeling, we point out that the pairwise volume-limited method works quite efficiently for faint galaxy samples with luminosity below  $L_*$ , while it leads to little improvement for luminous galaxy samples (above  $L_*$ ). We have verified this by comparing the faint-end volume-limited and pairwise volume-limited measurements for the  $M_r < -21$  sample. This difference between faint and bright galaxy samples results from the shape of the galaxy luminosity function. For luminosity  $L > L_*$ , the number density of galaxies drops exponentially towards the high luminosity end. Since the 2PCF component contribution from galaxies depends on their number density [equation (6)], the steep drop in the number density of brighter galaxies means that they only make a smaller contribution to the total 2PCF. Even their higher clustering amplitude cannot compensate the rapid (exponential) drop in their number density. For  $L < L_*$  galaxies, the number density change is not as steep (power-law rather than exponential), and the brighter galaxies in the sample can make a substantial contribution to the overall 2PCF. As a consequence, a better measurement of the clustering of brighter galaxies with the pairwise volume-limited method improves the overall 2PCF measurement.

#### 4 HOD MODELING OF THE CLUSTERING OF FAINT RED GALAXIES

With the pairwise volume-limited 2PCF measurements for the  $-19 < M_r < -18$  faint red galaxy sample, we perform HOD modeling to study the relationship between faint red galaxies and

dark matter haloes and discuss the implications for faint red galaxy formation. In our modeling, a halo is defined to have a mean density 200 times that of the background universe. We adopt a spatially flat cosmology with the following cosmological parameters,  $\Omega_m = 0.25$ ,  $\Omega_b = 0.043$ ,  $n_s = 0.95$ ,  $\sigma_8 = 0.8$ , and  $h = 0.7$ .

##### 4.1 HOD Parameterization

It is useful and physically meaningful to separate central galaxies and satellite galaxies in the HOD parameterization (Kravtsov et al. 2004; Zheng et al. 2005). We follow Z11 to construct the mean occupation function for the faint red galaxies as follows. Since we are modeling galaxies in a luminosity bin, the mean occupation function of central galaxies can be obtained by differencing those for two luminosity-threshold samples. The mean occupation function of central galaxies for a luminosity-threshold sample can be modeled as a softened step function (Zheng, Coil, & Zehavi 2007),

$$\langle N_{\text{cen}}(M) \rangle = \frac{1}{2} \left[ 1 + \text{erf} \left( \frac{\log M - \log M_{\text{min}}}{\sigma_{\log M}} \right) \right], \quad (8)$$

where  $M$  is the halo mass, erf is the error function,  $M_{\text{min}}$  is the characteristic minimum mass of haloes that can host the galaxies above the luminosity threshold, and  $\sigma_{\log M}$  characterizes the transition width of the softened step function (reflecting the scatter in the central galaxy luminosity and halo mass). We make use of the HOD modeling results in Z11 for the  $M_r < -18$  and  $M_r < -19$  sample and take the difference of the two corresponding central galaxy occupation functions. The shape (not the amplitude) of this difference central occupation function is used for the central occupation function for the  $-19 < M_r < -18$  faint red galaxies. The exact shape of the mean occupation function of central galaxies does not affect the modeling. This is because the role of the central galaxies is to contribute to the large scale bias and the number density. Since the mass of their host haloes is around a few times  $10^{11} h^{-1} M_\odot$ , where the halo bias reaches a plateau, the contributions to galaxy bias and number density from central galaxies are not sensitive to the shape of the mean occupation function.

For the satellite galaxies, we model the occupation function as a modified power law

$$\langle N_{\text{sat}}(M) \rangle = \left( \frac{M - M_0}{M_1} \right)^\alpha. \quad (9)$$

The satellite occupation number is assumed to follow a Poisson distribution with the above mean (Kravtsov et al. 2004; Zheng et al. 2005). We find that change in  $M_0$  does not affect our main results, so we first fix it at the value from the  $M_r < -18$  model (Z11) and follow Z11 to further modify  $N_{\text{sat}}(M)$  by the  $M_r < -18$  central occupation function. So our default model has  $M_1'$  and  $\alpha$  as free parameters, which characterize the amplitude and slope of the power law.

We use the shape from the above parameterization for the mean occupation functions of central and satellite galaxies, and the overall normalization of the mean occupation function for each set of HOD parameters is determined by the faint red galaxy number density. We start from assuming that the spatial distribution of satellites inside haloes follows the Navarro-Frenk-White (NFW) profile (Navarro et al. 1996), with the halo concentration parameter  $c(M) = c_0(1+z)^{-1}(M/M_{\text{nl}})^\beta$  (Bullock et al. 2001; Zhao et al. 2009), where  $c_0 = 11$ ,  $\beta = -0.13$ , and  $M_{\text{nl}} = 2.26 \times 10^{12} h^{-1} M_\odot$  is the non-linear mass scale at  $z = 0$ . Later in this section, we also show results with such an assumption relaxed.

The theoretical galaxy 2PCF in our model is calculated using

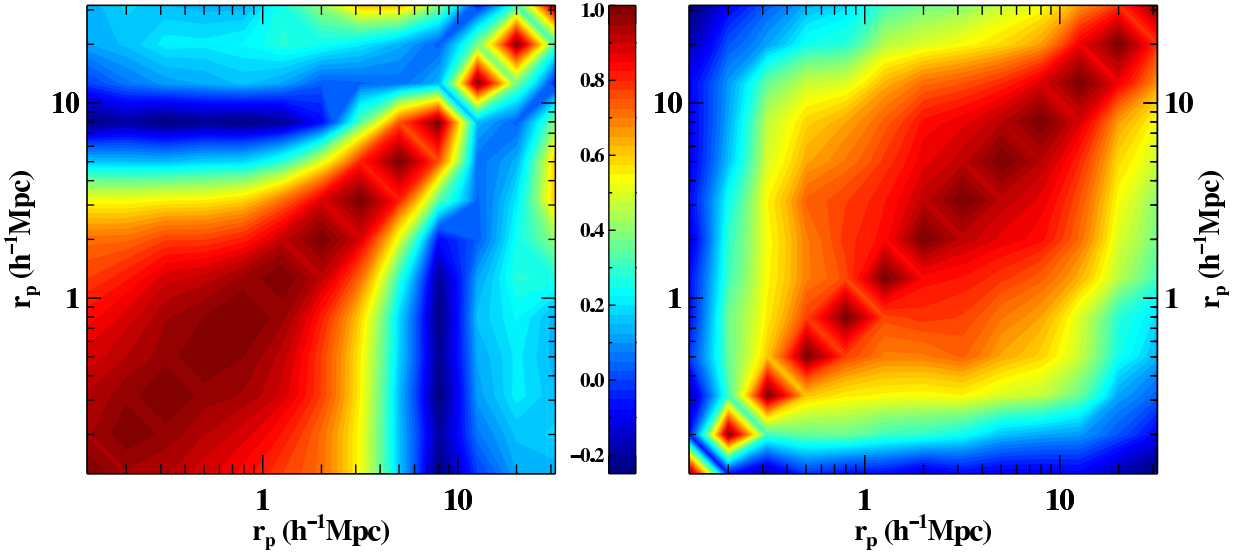


**Figure 4.** Covariance matrices of  $w_p$  for the  $-19 < M_r < -18$  red galaxies (left) and the  $M_r < -21$  sample (right). While the measurements for the bright sample are correlated on relatively large scales, those for the faint sample are highly correlated on small scales, suggesting a difference in the way that galaxies occupy haloes. See text for details.

the method described in Zheng (2004) and Tinker et al. (2005). In addition, we also incorporate the effect of residual redshift-space distortions when computing  $w_p$  from integrating the redshift-space 2PCF up to  $\pi_{\max}$  (instead of infinity), by applying the multipole expansion method of Kaiser (1987) (also see van den Bosch et al. 2013). A Markov Chain Monte Carlo (MCMC) method is adopted to explore the HOD parameter space constrained by the projected 2PCF  $w_p(r_p)$ .

#### 4.2 Modeling Results

Figure 5 shows the modeling result using the full covariance matrix (also shown as the 2-par HOD model in Figure 9). The default model leads to a reasonably good fit to the data. The best-fitting model has a value of  $\chi^2 = 18.0$  for 11 degrees of freedom (*dof*), which come from 13  $w_p$  data points and 2 free parameters ( $M_1'$  and  $\alpha$ ). Note that the number density  $n_g$  is not regarded as a data point but is only used to normalize the mean occupation function.

By eye, the best-fitting  $w_p$  works well on scales larger than  $4h^{-1}\text{Mpc}$ , but under-predicts the data on small scales, where the one-halo term dominates. However, given that the data points on small scales are highly correlated (Fig. 4), the deviation is not significant. We present the HOD constraints in other three panels. The mean occupation function (top-right panel) shows a bump for central galaxies around  $\log[M/(h^{-1}\text{M}_\odot)] = 11.3$  and a power law for satellite galaxies. The curve weighted by the differential halo mass function  $dn/d\log M$  is shown in the bottom-right panel ( $dp/d\log M = \langle N(M) \rangle dn/d\log M$ ), and we see that a randomly selected satellite faint red galaxy has comparable possibilities to reside in any haloes above a few times  $10^{11}h^{-1}\text{M}_\odot$ . The central galaxies has a large contribution to the galaxy bias factor and hence the 2PCF on large scales. The small-scale 2PCF is mainly contributed by satellite-satellite pairs in massive haloes. The frac-

tion of the faint red galaxies being satellites is above 70 per cent (bottom-left panel), even though such a high satellite fraction still makes the model  $w_p$  lie below the data points on small scales.

In the top-left panel of Figure 5, we also show as blue curves the predicted  $w_p$  from two best-fitting HOD models in Z11 (see the top-left panel of their Figure 21). The solid blue curve corresponds to the case with an HOD parameterization similar to ours. We find that their best-fitting model is able to reproduce our improved  $w_p$  measurements on large scales and the corresponding mean occupation function and satellite fraction ( $\sim 90$  per cent) is consistent with our constraints. It is interesting that this Z11 best-fitting HOD model “predicts” our improved  $w_p$  measurements on large scales, even though it is based on the original measurements with much lower amplitudes. The reason for this is that the small-scale  $w_p$  plays a significant role in determining the HOD. The dot-dashed blue curve is from an alternative model in Z11, where satellites are only allowed to populate massive haloes (above  $10^{13}h^{-1}\text{M}_\odot$ ) and there are more central galaxies in low-mass haloes in order to better match the low-amplitude large-scale  $w_p$  measurements in Z11. The corresponding mean occupation function of central galaxies (not shown in Figure 5 to avoid crowding) is about a factor of 5 higher than our best-fit. Clearly this alternative model underpredicts our improved large-scale  $w_p$  measurements.

To investigate the robustness of the HOD constraints, especially the high satellite fraction, we perform two model tests by exploring two possibilities, inaccurate covariance matrix and insufficient model.

Given the low luminosity nature of the sample under study, the survey volume is small,  $\sim 1.5 \times 10^6 h^{-3}\text{Mpc}^3$  for the faint-end volume-limited sample (e.g.  $\sim 30$  times smaller than that of the  $L > L_*$  sample). Even though our pairwise volume-limited measurements effectively increase the volume by a factor about two, it is still small (i.e., roughly corresponding to a cubic box with

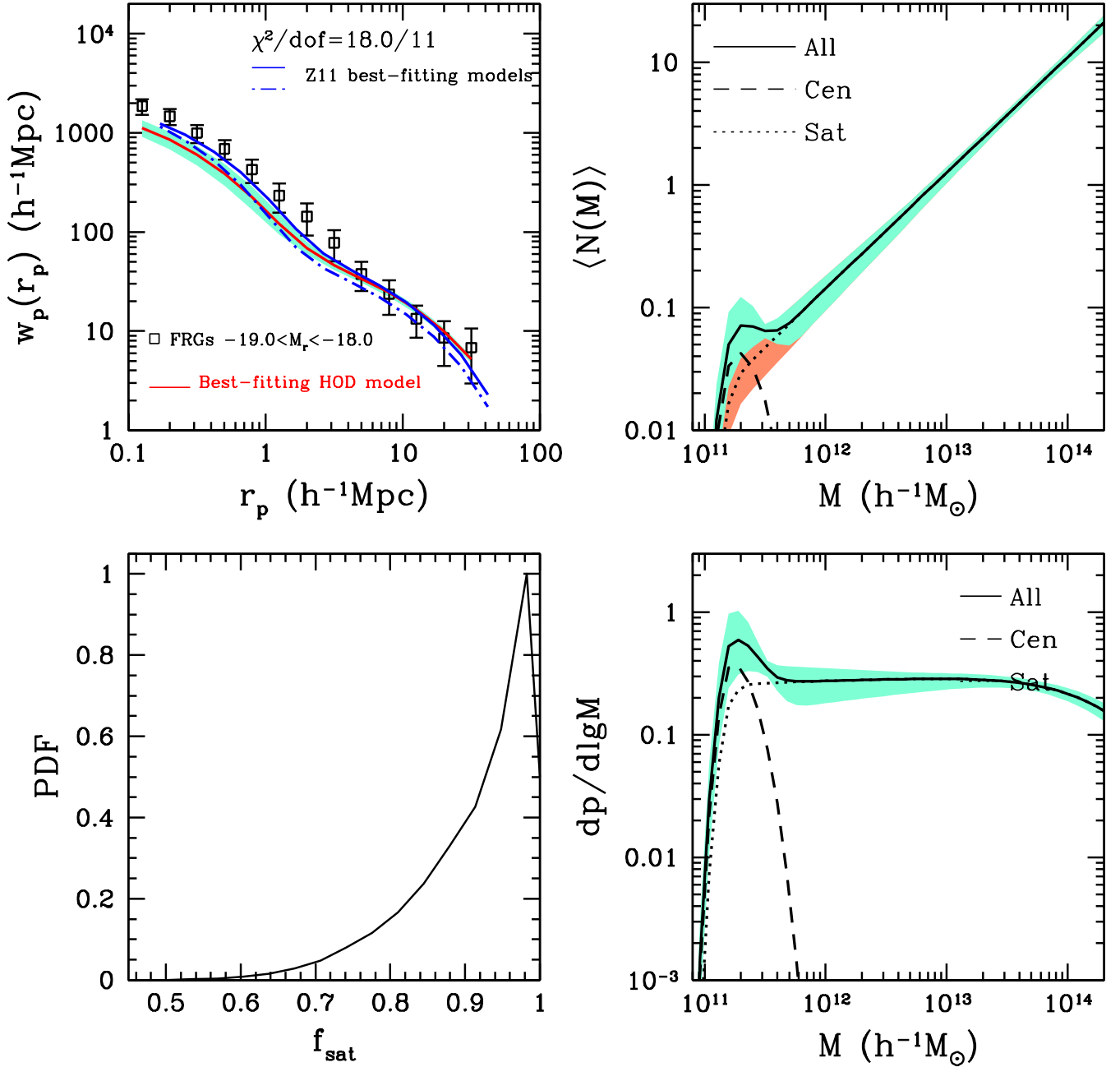


**Figure 5.** Results from modeling the pairwise volume-limited measurement of the projected 2PCF for the  $-19 < M_r < -18$  red galaxies. Full covariance matrix is used, and the default HOD model with two parameters are applied. *Top-left:* The measurement and the bestfit, with the shaded region indicating the range of model curves with the 68.3 per cent lowest values of  $\chi^2$ . For comparison, we overplot two best-fitting HOD models from Z11 as solid and dot-dashed blue curves (see text for details). *Top-right:* The inferred mean occupation functions, with the shaded region having the similar meaning as above. *Bottom-right:* The probability distribution of mass of the host haloes, obtained by multiplying the curve in the top-right panel with the differential halo mass function. *Bottom-left:* The marginalized distribution of the fraction of faint red galaxies being satellites.

$150h^{-1}\text{Mpc}$  on a side). The covariance matrix estimated from the small volume may not be accurate. Noises in the covariance matrix can affect the value of  $\chi^2$  and the constraints. Compared to the covariance between data points at different values of  $r_p$ , the diagonal elements of the covariance matrix are more reliably determined. We perform a test by using only the diagonal elements in the fit.

A perfect fit is achieved, with the best-fitting  $\chi^2/\text{dof} = 4.5/11$ . The fit to small-scale data points is improved by populating more satellites into more massive haloes, i.e., a higher high-mass

end slope  $\alpha$  of the satellite mean occupation function. A larger fraction of satellites reside in haloes above  $10^{13}h^{-1}\text{M}_\odot$ . Compared to the fit with the full covariance matrix, the overall satellite fraction shows a bimodal distribution, peaked around  $\sim 25$  per cent and  $\sim 70$  per cent. This test with diagonal errors of the covariance matrix shows that the noises in the covariance matrix may affect the best-fitting  $\chi^2$ , but satellites in massive haloes are necessary to explain the strong small scale clustering. Since this model neglects the



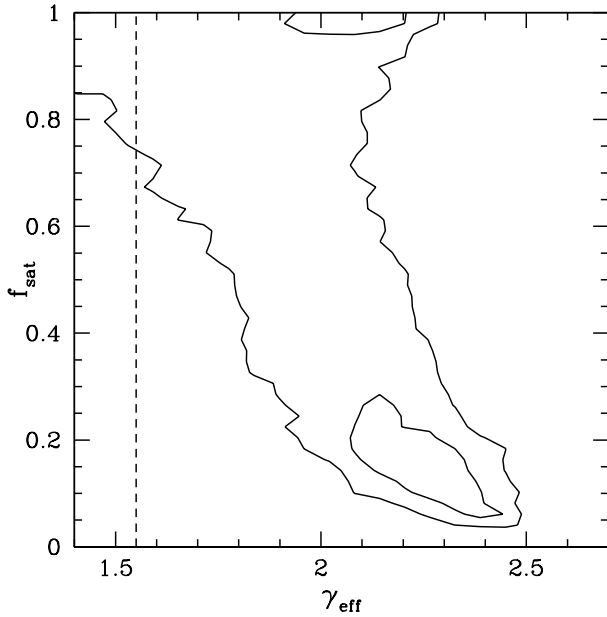


**Figure 6.** Marginalized distribution of satellite fraction and effective slope of inner profile of satellite distribution. The effective slope of a generalized NFW profile is computed at  $r = 0.1h^{-1}\text{Mpc}$  in haloes of mass  $2 \times 10^{14}h^{-1}\text{M}_{\odot}$ . See text for detail. The contours represent the 68.3 per cent and 95.5 per cent confidence levels. The vertical dash line marks  $\gamma_{\text{eff}} = 1.55$ , the value corresponding to slope of the NFW profile at this radius.

strong correlation among small-scale data points, the results should be taken with a grain of salt.

Next, we add more flexibility in the model by allowing the spatial distribution of satellites to deviate from the NFW profile. A generalized NFW profile is adopted, with the concentration parameter  $c$  and inner slope  $\gamma$  as two additional free parameters (e.g. [Watson et al. 2010, 2012](#); [van den Bosch et al. 2013](#); [Guo et al. 2014](#)),

$$\rho(r) \propto \left[ \left( \frac{cr}{r_{\text{vir}}} \right)^{\gamma} \left( 1 + \frac{cr}{r_{\text{vir}}} \right)^{3-\gamma} \right]^{-1}, \quad (10)$$

where  $r_{\text{vir}}$  is the halo virial radius. The modeling results with the full covariance matrix is shown in Figure 9, termed as the *4-par HOD model*. The best-fitting  $\chi^2 = 14.9/9$  is reasonable. The model still under-predicts the small-scale clustering, but these data points are highly correlated. The mean occupation function is similar to the case with diagonal covariance matrix, but with a much large spread. The fit shows a bimodal distribution, favoring either a high satellite fraction ( $>70$  per cent) or a steeper inner profile. To illustrate this, in Figure 6, we show the marginalized distribution of the derived satellite fraction  $f_{\text{sat}}$  and the effective inner slope  $\gamma_{\text{eff}}$ . We choose to compute the effective slope at  $r = 0.1h^{-1}\text{Mpc}$  in haloes of mass  $2 \times 10^{14}h^{-1}\text{M}_{\odot}$ ,

$$\gamma_{\text{eff}} \equiv -\frac{d \ln \rho(r)}{d \ln r} = \gamma + \frac{c(3-\gamma)}{c + r_{\text{vir}}/r}. \quad (11)$$

For comparison, the vertical dashed line shows the effective slope for the corresponding NFW profile ( $\gamma = 1$ ).

The steeper inner profile helps enhance the small-scale clustering, and thus reduces the need for a high satellite fraction (only need  $f_{\text{sat}} \sim 20$  per cent). If the diagonal covariance matrix were used with the generalized NFW profile, the fit would have best-

fitting  $\chi^2/\text{dof} = 2.0/9$ , and the satellite fraction is close to a uniform distribution from  $\sim 20$  per cent to  $\sim 100$  per cent.

If we further allow the cutoff mass  $M_0$  in the satellite mean occupation function to float, the way to populate satellites becomes even more degenerate, ranging from solutions similar to the above cases to those with satellite galaxies only populating very massive haloes (e.g. above  $10^{13.5}h^{-1}\text{M}_{\odot}$ ).

From the above modeling results and various tests, we find that the satellite fraction is degenerate with the spatial distribution profile of satellites. For a profile not far from NFW, the strong small-scale clustering requires a large fraction of the faint red galaxies to be satellite galaxies in high mass haloes. Even with steep inner profiles, a fraction of faint red galaxies are still needed to be satellites in high mass haloes.

Breaking the degeneracy between the high satellite fraction and the steep inner profile needs additional information. The pattern seen in the covariance matrix (left panel of Figure 4) in fact supports the solution that at least a considerable fraction of faint red galaxies need to be satellites in massive haloes. The strong correlation occurs for data points that are dominated by contributions from intra-halo satellite-satellite pairs in massive haloes, so the clustering amplitude on such scales is sensitive to the number of massive haloes within the given (survey) volume. The covariance matrix reflects the covariance of the measurements across different regions (of the same volume) in the universe (or ‘same’ region in different realizations of the universe). Such a sample variance effect affects more the number of massive haloes than that of low mass haloes. That is, the number of massive haloes fluctuates more than that of low-mass haloes across different regions. In slightly denser regions, we expect to have more haloes of higher masses, which increases the number of intra-halo satellite-satellite pairs and thus enhances the small-scale clustering (over all relevant one-halo scales simultaneously). In regions of lower density, we have the opposite effect that the small-scale clustering becomes weaker simultaneously. This explains the relatively strong correlation among small-scale data points. On the contrary, the large-scale clustering has a large contribution from faint red galaxies residing in haloes of a few times  $10^{11}h^{-1}\text{M}_{\odot}$  (as central galaxies). The abundance of such low-mass haloes does not fluctuate much across different regions of the above volume, and therefore a strong correlation is not seen among the large-scale data points.

A considerable fraction of the faint red galaxies being satellites in massive haloes can help explain the high pairwise velocity dispersion inferred from small scales ([Li et al. 2006b](#)) and small-scale redshift-space distortions ([Ross et al. 2011](#)). The need for satellites is also supported by a visual check of the spatial distribution in a slice of volume, as shown in Figure 7. The red dots are  $-19 < M_r < -18$  red galaxies. The filled and open black circles are more luminous galaxies, displaying the locations of high mass haloes ( $\log M \gtrsim 12.8$  for  $M_r < -21$  and  $\log M \gtrsim 13.4$  for  $M_r < -21.5$ ; see Z11). A large fraction of the faint red galaxies are found close to these high mass haloes residing in over-dense regions, suggesting a high probability of being satellites. However, there are also faint red galaxies in the ‘void’ regions in the diagram, which means that a fraction of them can be central galaxies of low mass haloes. This is consistent with the mean occupation function having both central and satellite components, as in our HOD model.

The visual impression of a high probability of faint red galaxies being satellites in Figure 7 can be further justified by counting the correlated pairs of faint and luminous galaxies, which also helps remove the confusion from chance alignment. Figure 8 shows the mean excess surface density of faint red galaxies ( $-19 < M_r <$

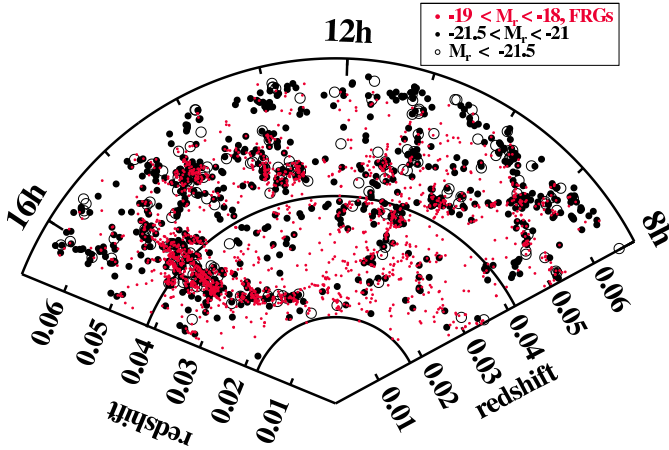


**Figure 7.** Comparison between the spatial distributions of faint red galaxies and more luminous galaxies. The slice is chosen to be around the celestial equator with declination in the range of  $|\delta| < 10^\circ$ . The two inner arcs ( $0.017 < z < 0.042$ ) marks the boundary for the faint-end volume-limited  $-19 < M_r < -18$  sample.

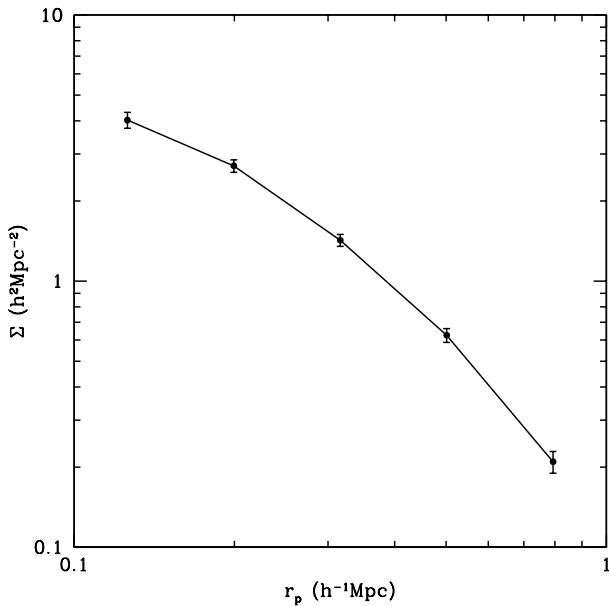


**Figure 8.** Mean excess surface density of faint red galaxies ( $-19 < M_r < -18$ ) around one luminous galaxies with  $M_r < -21$ . Poisson error bars are plotted.

$-18$ ) per luminous galaxy with  $M_r < -21$  as a function of the projected distance to the luminous galaxy, from counting faint red galaxies within  $\Delta\pi = \pm 30 h^{-1} \text{Mpc}$  of luminous galaxies. This is done in the volume where the faint galaxies are complete and is equivalent to the cross-correlation function between faint red and luminous galaxies. Since the majority of  $M_r < -21$  galaxies are central galaxies ( $\sim 91$  per cent; see Z11), the excess faint red galaxies are almost all satellite galaxies. From the above density profile and the number density of luminous galaxies, we can infer the number density of faint red galaxies within a projected distance  $1 h^{-1} \text{Mpc}$  away from luminous galaxies, which is about 56 per cent of all faint red galaxies. As a rough estimate of the fraction of

(satellite) faint red galaxies in host haloes of  $M_r < -21$  galaxies, this number is close to the satellite fraction (about 45 per cent) in  $M_r < -21$  host haloes inferred from our best-fitting HOD model of faint red galaxies and the halo mass distribution of  $M_r < -21$  galaxies (Z11). Our result that most faint red galaxies are satellites is therefore well supported.

Finally, we compare our modeling results with predictions from the semi-analytic model (SAM) of galaxy formation in Guo et al. (2013). More specifically, we construct the faint red galaxies sample with the MS-SW7 SAM catalog (WMAP7 cosmology), by adopting the same luminosity and colour cut as used in defining our faint red galaxy sample. The mock sample has a number density of  $1.46 \times 10^{-3} h^3 \text{Mpc}^{-3}$ , about 40 per cent that of the observed sample. The SAM predicted  $w_p$  is shown in the left panel of Figure 9, together with the range of model fits from the default 2-parameter and the 4-parameter HOD models. On scales above  $1 h^{-1} \text{Mpc}$ , the prediction falls on top of the data. However, the SAM clearly over-predicts  $w_p$  below  $1 h^{-1} \text{Mpc}$ , as noted by Guo et al. (2013). The SAM prediction also appears to have a steeper slope than the data points. To be quantitative, the  $\chi^2$  calculated from comparing the SAM curve with the data points is 778.3, which is a poor fit.

The SAM predicted mean occupation function is shown in the right panel of Figure 9. Encouragingly, it has the similar central component (a bump around  $\log M = 11.3$ ) and satellite component (roughly following a power law) as inferred from the HOD modeling. The satellite mean occupation function has a similar slope as in our default model with two parameters (blue). It then implies that the SAM would predict a similar small-scale slope in  $w_p$  as the HOD model. However, the SAM leads to a steeper slope as seen in the left panel, which means that the inner spatial distribution of SAM satellites is too steep. In Figure 10, we compare the spatial distribution of SAM satellites and the NFW profile, stacked with haloes of masses above  $10^{13} h^{-1} M_\odot$  and radius normalized to halo virial radius. The scales relevant to the measurements ( $r_p > 0.1 h^{-1} \text{Mpc}$ ) correspond to  $r/R_{\text{vir}} \gtrsim 0.2$ , and clearly the SAM satellites show a much steeper profile than the NFW profile used in our modeling. We also find that the SAM predicts a satellite fraction of 35 per cent, and it lies in the middle of the two extreme solutions with the 4-parameter HOD model (in between high satellite fraction and very steep inner profile). The steep rise in  $w_p$  towards small scales from SAM suggests that its predicted combination of satellite fraction and inner distribution profile deviates from that implied by the data.

As for the physical origin of the over-prediction of the small-scale clustering by the SAM model, Guo et al. (2013) attribute it to the over-abundance of low-mass galaxies and/or galaxies forming too early. This is supported by the results that the stellar mass and luminosity functions of satellites and the radial distribution of satellites around primary galaxies in the SAM model match those observed in the SDSS, while large discrepancies show up when split by color, with red satellites being over-predicted (Wang & White 2012; Wang et al. 2014), pointing the origin to the quenching of satellites. Modifying baryon processes and environmental effects can make significant improvements (Henriques et al. 2015). For the particular faint red galaxy population we study here, the SAM model underpredicts the satellite fraction, compared to the HOD modeling results.

From such a comparison, the steeper slope in the spatial distribution of SAM satellites indicates that the SAM implementation may shut off star formation in faint satellites too late in massive haloes, making them more concentrated toward the halo centre, or

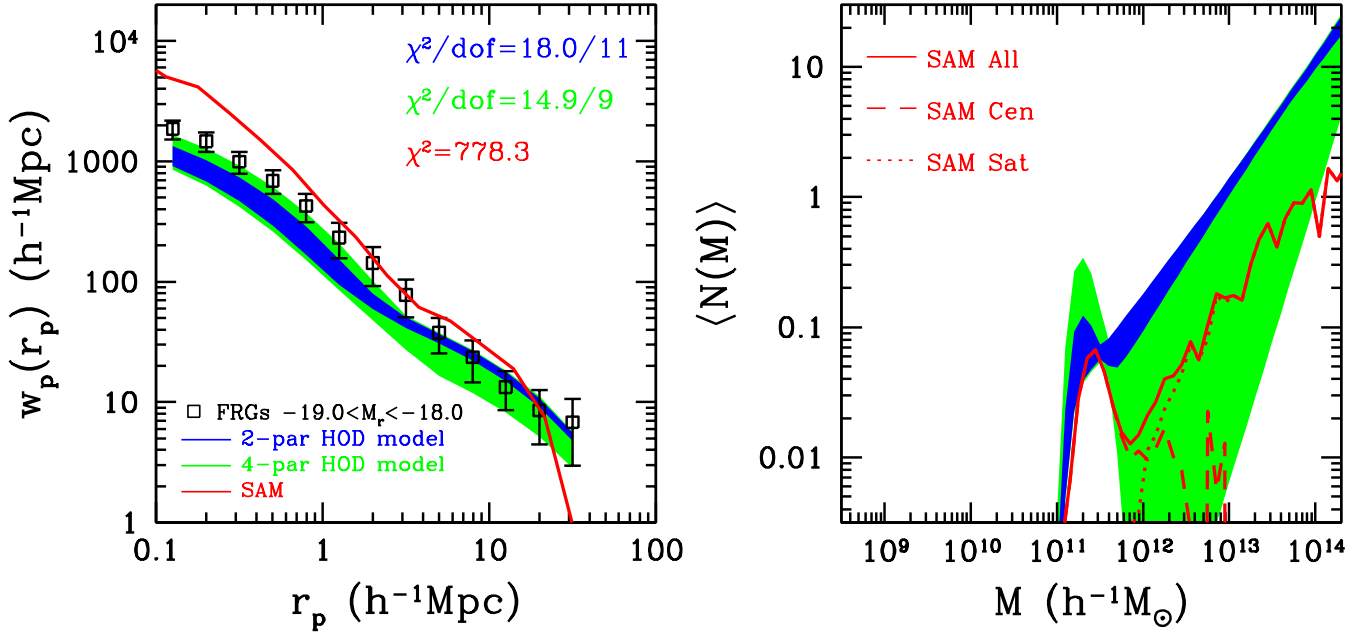


**Figure 9.** Comparison between two HOD modeling results and the SAM prediction for the clustering and mean occupation functions of the  $-19 < M_r < -18$  red galaxies. The 2-par HOD model has the amplitude ( $M'_1$ ) and slope ( $\alpha$ ) in the power law of satellite mean occupation function as free parameters, while the 4-par HOD model adopts a generalized NFW profile for satellite distribution inside haloes, adding the concentration ( $c$ ) and inner density slope ( $\gamma$ ) as two additional parameters. See text in detail. Green and blue shaded region shows the envelopes from models with the 68.3 per cent lowest values of  $\chi^2$ .

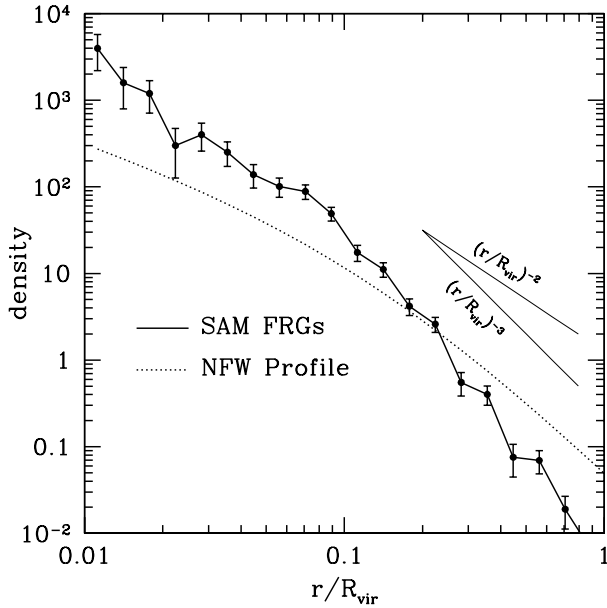


**Figure 10.** Comparison between the spatial distribution of SAM faint red satellites and the NFW profile in massive haloes. Both profiles are obtained by stacking haloes above  $10^{13} h^{-1} M_\odot$  with radius normalized to halo virial radius. Two straight solid lines mark two power-law profiles with different slopes to guide the eye.

that the efficiency of disrupting faint red galaxies toward the halo centre or merging them with the central galaxy is too low in the SAM model.

## 5 SUMMARY AND DISCUSSION

We introduce a method to improve the volume-limited 2PCF measurements of faint galaxies by making a full use of the flux-limited sample. The method is then applied to the  $-19 < M_r < -18$  SDSS red galaxies to obtain a more accurate projected 2PCF measurement, and we perform HOD modeling to infer the relation between these faint red galaxies and dark matter haloes.

The depth of a galaxy redshift survey limits the observation of faint galaxies, which cannot be observed to large redshifts. For the ease of interpretation, the clustering of faint galaxies is usually studied with a small, volume-limited sample, giving rise to considerable sample variance. The method introduced in this work (termed as ‘pairwise volume-limited measurement’), when applied to luminosity-bin or luminosity-threshold galaxy samples, decomposes the galaxy pair contribution to correlations of pairs with same or different luminosities. Each pair count is made volume-limited, by weighing with the appropriate volume factor (i.e. common volume of being complete for both galaxies). It shares some similarity with the  $1/V_{\max}$  method to estimate galaxy luminosity function. The final form of the method is a generalized Landy-Szalay estimator. The method uses all possible pairs in a flux-limited sample to form an effectively volume-limited measurements. With the contribution to the 2PCF from more luminous galaxies in the sample measured in a larger volume, we effectively increase the sample volume (by a factor of about two). As a consequence, the uncertainty in the 2PCF measurements can be improved (by tens of per cent) and the effect of sample variance is reduced. Since galaxy luminosity function drops exponentially above  $L_*$ , the method turns out to be most efficient for samples of faint galaxies (with luminosity below  $L_*$ ).

We apply the method to the  $-19 < M_r < -18$  SDSS red galaxies and make the pairwise volume-limited projected 2PCF measurements. Compared to those from the commonly used

volume-limited sample, the improved measurements have  $\sim 40$  per cent smaller uncertainties on large scales. Furthermore, the previous puzzling result that the sample shows a strong small-scale clustering and a weak large-scale clustering (Z11) is not seen in the improved measurements. Suffering less from the effect of sample variance, the measured  $w_p$  shows a more consistent trend from small to large scales. In addition, we also apply the method to all the  $-19 < M_r < -18$  galaxies (red+blue) and measure the large-scale galaxy bias factor from the ratio of the measured  $w_p$  to that of the dark matter. Compared to the bias factor  $0.90 \pm 0.10$  inferred in Z11 (left panel of their Fig.7), we find the updated value to be  $0.99 \pm 0.12$ , much more consistent with the value derived from HOD modeling.

With the previous volume-limited measurements, it was difficult for HOD modeling to simultaneously reproduce the strong small-scale clustering and the weak large-scale clustering. As a possible explanation of the data, Z11 invoke a scenario to put satellites only in haloes above  $10^{13} h^{-1} M_\odot$  and have central galaxies in haloes of a few times  $10^{11} h^{-1} M_\odot$ . The motivation is that gas accretion and star formation in satellites shut off more efficiently in haloes more massive than the previous host haloes of those satellites before they are accreted into the haloes (e.g. Font et al. 2008; Kang & van den Bosch 2008; Simha et al. 2009). With our improved measurements, in particular those on large scales, we find that the above scenario is not necessary in explaining the data with our simple two-parameter model, but remains a possibility for the more flexible model. With the two-parameter model, a reasonable fit to the data can be achieved and we find that the faint red satellites can reside in haloes ranging from a few times  $10^{11} h^{-1} M_\odot$  to cluster-size haloes more massive than  $10^{14} h^{-1} M_\odot$ , leading to large satellite fraction ( $> 70$  per cent). Unsurprisingly, with the more flexible, four-parameter model, we find that a steep inner profile of the spatial distribution of satellites inside haloes can compensate the high satellite fraction. However, either solution needs to put a fraction of satellites in massive haloes. Such a picture is supported by the strong covariance among small-scale data points and by the relative spatial distribution of the faint red galaxies and more luminous galaxies tracing massive haloes.

The mean occupation function of those faint red galaxies predicted in the SAM model of Guo et al. (2013) falls into the range of our model constraints. However, the predicted small-scale clustering appears to be too strong to be consistent with the measurements, indicating a too steep inner distribution profile of satellites in the SAM model. It suggests that the disruption or merging of faint red galaxies in massive haloes are more efficient than that implemented in the SAM model.

Although we develop a method to make more accurate volume-limited measurements of faint galaxy clustering, we still lack very tight HOD constraints and could not draw too strong a conclusion regarding the nature of the faint red galaxies. This limits the power of the 2PCF measurements to efficiently assess the effects like assembly bias (e.g. Zentner et al. 2014). The role of assembly bias in the clustering of faint red galaxies deserves a further investigation. Combining the 2PCFs with other statistics, like those from group catalogs (e.g. Skibba 2009; Wang et al. 2009), can be helpful. A deep and large survey probably is the ultimate resort to using clustering to study the faint galaxy population.

## ACKNOWLEDGEMENTS

We thank Cheng Li and David Weinberg for helpful discussions and Simon White for useful comments. HJX thanks Yiping Shu for technical help. ZZ is partially supported by NSF grant AST-1208891 and NASA grant NNX14AC89G. IZ and ZZ also acknowledge NSF grant AST-0907947.

Funding for the Sloan Digital Sky Survey (SDSS) has been provided by the Alfred P. Sloan Foundation, the Participating Institutions, the National Aeronautics and Space Administration, the National Science Foundation, the U.S. Department of Energy, the Japanese Monbukagakusho, and the Max Planck Society. The SDSS Web site is <http://www.sdss.org/>.

The SDSS is managed by the Astrophysical Research Consortium (ARC) for the Participating Institutions. The Participating Institutions are The University of Chicago, Fermilab, the Institute for Advanced Study, the Japan Participation Group, The Johns Hopkins University, Los Alamos National Laboratory, the Max-Planck-Institute for Astronomy (MPIA), the Max-Planck-Institute for Astrophysics (MPA), New Mexico State University, University of Pittsburgh, Princeton University, the United States Naval Observatory, and the University of Washington.

## References

- Abazajian K. N. et al., 2009, *ApJS*, 182, 543
- Adelman-McCarthy J. K. et al. 2008, *ApJS*, 175, 297
- Berlind A. A., Weinberg D. H., 2002, *ApJ*, 575, 587
- Blanton M. R., Eisenstein D., Hogg D. W., Schlegel D. J., Brinkmann, J. 2005a, *ApJ*, 629, 143
- Blanton M. R. et al. 2005b, *AJ*, 129, 2562
- Bullock J. S., Kolatt T. S., Sigad Y., Somerville R. S., Kravtsov A. V., Klypin A. A., Primack J. R., Dekel A., 2001, *MNRAS*, 321, 559
- Cresswell J. G., Percival W. J. 2009, *MNRAS*, 392, 682
- Fisher K. B., Davis M., Strauss M. A., Yahil A., Huchra J. 1994, *MNRAS*, 266, 50
- Font A. S. et al. 2008, *MNRAS*, 389, 1619
- Guo Q., White S., Angulo R. E., Henriques B., Lemson G., Boylan-Kolchin M., Thomas P., Short C., 2013, *MNRAS*, 428, 1351
- Guo H. et al. 2014, *MNRAS*, 441, 2398
- Henriques B. M. B., White S. D. M., Thomas P. A., Angulo R., Guo Q., Lemson G., Springel V., Overzier R., 2015, *MNRAS*, 451, 2663
- Hogg D. W. et al. 2003, *ApJL*, 585, L5
- Huchra J. P., Sargent W. L. W. 1973, *ApJ*, 186, 433
- Jing Y. P., Mo H. J., Börner G., 1998, *ApJ*, 494, 1
- Kaiser N., 1987, *MNRAS*, 227, 1
- Kang X., van den Bosch F. C. 2008, *ApJL*, 676, L101
- Kravtsov A. V., Berlind A. A., Wechsler R. H., Klypin A. A., Gottlöber S., Allgood B., Primack J. R., 2004, *ApJ*, 609, 35
- Landy S. D., Szalay A. S. 1993, *ApJ*, 412, 64
- Li C., Kauffmann G., Jing Y. P., White S. D. M., Brner G., Cheng F. Z., 2006a, *MNRAS*, 368, 21
- Li C., Jing Y. P., Kauffmann G., White S. D. M., Brner G., Cheng F. Z., 2006b, *MNRAS*, 368, 37
- Li C., White S. D. M. 2009, *MNRAS*, 398, 2177
- Li C., White S. D. M., Chen Y., Coil A. L., Davis M., De Lucia G., Guo Q., Jing Y. P., Kauffmann G., Willmer C. N. A., Zhang W., 2012, *MNRAS*, 419, 1557
- Navarro J. F., Frenk C. S., White S. D. M. 1996, *ApJ*, 462, 563
- Norberg P., et al. 2002, *MNRAS*, 332, 827
- Padmanabhan N., et al. 2008, *ApJ*, 674, 1217
- Peacock J. A., Smith R. E., 2000, *MNRAS*, 318, 1144
- Peebles P. J. E. 1980, *The large-scale structure of the universe*
- Ross A. J., Tojeiro R., Percival W. J. 2011, *MNRAS*, 413, 2078
- Schmidt M., 1968, *ApJ*, 151, 393



- Scoccimarro R., Sheth R. K., Hui L., Jain B., 2001, *ApJ*, 546, 20
- Seljak U., 2000, *MNRAS*, 318, 203
- Simha V., Weinberg D. H., Davé R., Gnedin O. Y., Katz N., Kereš D., 2009, *MNRAS*, 399, 650
- Skibba R. A. 2009, *MNRAS*, 392, 1467
- Stoughton C., et al. 2002, *AJ*, 123, 485
- Strauss M.A., et al. 2002, *AJ*, 124, 1810
- Swanson M. E. C., Tegmark M., Blanton M., Zehavi I. 2008, *MNRAS*, 385, 1635
- Tinker J. L., Weinberg D. H., Zheng Z., Zehavi I., 2005, *ApJ*, 631, 41
- van den Bosch F. C., More S., Cacciato M., Mo H., Yang X., 2013, *MNRAS*, 430, 725
- Wang W., White S. D. M., 2012, *MNRAS*, 424, 2574
- Wang W., Sales L. V., Henriques B. M. B., White S. D. M., 2014, *MNRAS*, 442, 1363
- Wang Y., Yang X., Mo H. J., van den Bosch F. C., Katz, N., Pasquali, A., McIntosh, D. H., Weinmann S. M., 2009, *ApJ*, 697, 247
- Watson D. F., Berlind A. A., McBride C. K., Hogg D. W., Jiang T., 2012, *ApJ*, 749, 83
- Watson D. F., Berlind A. A., McBride C. K., Masjedi M., 2010, *ApJ*, 709, 115
- Yang X., Mo H. J., van den Bosch F. C., 2003, *MNRAS*, 339, 1057
- York D. G., et al. 2000, *AJ*, 120, 1579
- Zehavi I. et al., 2005, *ApJ*, 621, 22
- Zehavi I., et al. 2011, *ApJ*, 736, 59
- Zentner A. R., Hearin A. P., van den Bosch F. C. 2014, *MNRAS*, 443, 3044
- Zhao D. H., Jing Y. P., Mo H. J., Börner G., 2009, *ApJ*, 707, 354
- Zheng Z. 2004, *ApJ*, 610, 61
- Zheng Z., et al. 2005, *ApJ*, 633, 791
- Zheng Z., Coil A. L., Zehavi I. 2007, *ApJ*, 667, 760
- Zu Y., Zheng Z., Zhu G., Jing Y. P. 2008, *ApJ*, 686, 41
- Zu Y., Mandelbaum R. 2015, *MNRAS*, 454, 1161

## APPENDIX A: GENERALIZED LANDY-SZALAY ESTIMATOR FOR PAIRWISE VOLUME-LIMITED GALAXY 2PCF MEASUREMENT

Here we derive the expression for the pairwise volume-limited galaxy 2PCF measurement from a flux-limited galaxy sample.

First, consider a volume-limited sample of galaxies in a luminosity bin  $[L_0, L_N]$ . We divide it into  $N$  subsamples of fine luminosity bins,  $[L_0, L_1], [L_1, L_2], \dots, [L_{N-1}, L_N]$  ( $L_0 < L_1 < \dots < L_N$ ). The 2-point auto-correlation function  $\xi$  of the whole sample can then be decomposed into contributions from the 2-point auto-correlation function  $\xi_{ii}$  ( $i = 1, 2, \dots, N$ ) of each subsample and the 2-point cross-correlation functions  $\xi_{ij}$  ( $i, j = 1, 2, \dots, N$ ;  $i \neq j$ ) among different subsamples (Zu et al. 2008),

$$\xi = \sum_{i,j} \frac{\bar{n}_i \bar{n}_j}{\bar{n}^2} \xi_{ij}, \quad (\text{A1})$$

where  $\bar{n}_i$  is the mean number density of the  $i$ -th subsample and  $\bar{n} = \sum \bar{n}_i$  is that of the whole sample. This is just a reflection that the total number of pairs is the sum over all possible auto-pairs ( $i$ - $i$ ) and cross-pairs ( $i$ - $j$ ). Note that in the summation, both  $i$  and  $j$  go from 1 to  $N$ , hence no coefficient 2 in front of the cross-correlation terms.

For a flux-limited sample of galaxies with the same luminosity range  $[L_0, L_N]$ , we can do the same division into subsamples of fine luminosity bins. Each subsample has its own corresponding maximum volume that makes it volume-limited, i.e., the subsample of galaxies are complete within this volume. Denote  $V_i$  as such a volume for the  $i$ -th subsample. To compute the 2PCF of galaxies in the  $[L_0, L_N]$  bin in a volume-limited sense, equation (A1) still applies, but we can evaluate  $\xi_{ij}$  in a volume that both the  $i$ -th

subsample and  $j$ -th subsample are complete. Denote the common volume as  $V_{ij}$ . Obviously  $V_{ij} = \min\{V_i, V_j\}$ , determined by the fainter subsample of the two. The correlation function  $\xi_{ij}$  can be calculated using the Landy-Szalay estimator in the volume  $V_{ij}$ ,

$$\xi_{ij} = \frac{DD_{ij} - 2DR_{ij} + RR_{ij}}{RR_{ij}} \bigg|_{V_{ij}}, \quad (\text{A2})$$

where  $DD_{ij}$ ,  $DR_{ij}$ , and  $RR_{ij}$  are the numbers of  $i$ - $j$  data-data, data-random, and random-random pairs. For measuring the correlation function at pair separation  $\mathbf{r}$  [e.g.  $(r_p, \pi)$ ], each of the above pair counts should be understood as the number of pairs with separation within a bin  $d\mathbf{r}$  around  $\mathbf{r}$  (i.e.,  $\mathbf{r} \pm d\mathbf{r}/2$ ). For the simplicity of the derivation later, we assume the same number of data and random points, so we do not need to normalize those pair counts. We also note that the random catalog should be constructed in a way that each random point is assigned a luminosity, drawn randomly from the luminosity distribution of the galaxy sample. That is, at any small luminosity bin, random points have the same redshift distribution and volume of completeness as the galaxy sample.

Now let us take a look at the weight in equation (A1), which is determined by the subsample number densities. We can link the number densities to pair counts from the random catalog. For pairs composed of random points in the  $i$ -th and  $j$ -th luminosity bins, we can compute the counts  $RR_{ij}(\mathbf{r})|_{V_{ij}}$  of  $i$ - $j$  pairs with separation  $\mathbf{r} \pm d\mathbf{r}/2$  in the common volume  $V_{ij}$  of completeness. Under the condition  $r^3 \ll V_{ij}$ , the counts are simply the product of the number of  $j$ -luminosity points in a volume  $dV = d^3\mathbf{r}$  with separation  $\mathbf{r}$  from each  $i$ -luminosity points and the total number of  $i$ -luminosity points in volume  $V_{ij}$ , with the former  $\bar{n}_j dV$  and the latter  $\bar{n}_i V_{ij}$ , i.e.

$$RR_{ij}(\mathbf{r})|_{V_{ij}} = \bar{n}_i \bar{n}_j V_{ij} dV. \quad (\text{A3})$$

We then have

$$\bar{n}_i \bar{n}_j = \frac{1}{dV} \frac{1}{V_{ij}} RR_{ij}(\mathbf{r})|_{V_{ij}}. \quad (\text{A4})$$

From  $\bar{n} = \sum \bar{n}_\alpha$ ,  $\bar{n}^2$  can be expressed as  $\bar{n}^2 = \sum_{\alpha,\beta} \bar{n}_\alpha \bar{n}_\beta$  ( $\alpha, \beta = 1, 2, \dots, N$ ). Substituting equation (A4) into the expression, we have

$$\bar{n}^2 = \frac{1}{dV} \sum_{\alpha,\beta} \frac{1}{V_{\alpha\beta}} RR_{\alpha\beta}(\mathbf{r})|_{V_{\alpha\beta}}. \quad (\text{A5})$$

Substituting equations (A2), (A4), and (A5) into equation (A1) results in

$$\xi(\mathbf{r}) = \frac{\sum_{i,j} \frac{1}{V_{ij}} [DD_{ij}(\mathbf{r}) - 2DR_{ij}(\mathbf{r}) + RR_{ij}(\mathbf{r})]|_{V_{ij}}}{\sum_{i,j} \frac{1}{V_{ij}} RR_{ij}(\mathbf{r})|_{V_{ij}}}. \quad (\text{A6})$$

This equation provides a generalization to the Landy & Szalay estimator, which can be applied to flux-limited sample to make effectively volume-limited galaxy 2PCF measurements. The derivation assumes the same number of data and random points. In practice, the random sample is much larger than the data sample. In such a case, it is easy to show that one needs to use the normalized pair counts,  $DD_{ij}$ ,  $DR_{ij}$ , and  $RR_{ij}$ .

The estimator in equation (A6) states that the pair counts are weighted by  $1/V_{ij}$ , where  $V_{ij}$  is the common volume that both galaxies in the  $i$ -th and  $j$ -th luminosity bins are complete. This is similar to the  $1/V_{\text{max}}$  method of estimating the galaxy luminosity function from a flux-limited sample. In practice, we do not need to divide the sample into finite luminosity bins — for each pair

(data-data, data-random, or random-random), if both members of the pair fall into the common volume  $V$  of completeness determined by the fainter member, we keep the pair and give it a weight  $1/V$ . We note that a similar  $1/V$  weight to galaxy pairs has been adopted by Li et al. (2006a), Li & White (2009) and Li et al. (2012) in estimating the distribution of stellar mass in the universe and the stellar-mass-dependent galaxy 2PCFs. While  $V$  is also defined as the lower  $V_{\max}$  of the two galaxies of each pair, there is a subtle difference between our method and theirs in how the weight is applied. They apply the weight to all galaxy pairs, including also galaxy pairs with one galaxy inside  $V$  and the other outside  $V$ . However, in our method based on a formal derivation of the modified LS estimator from the perspective of decomposing the 2PCF, we do not count such galaxy pairs in measuring the 2PCFs. Our method implicitly assumes that the two galaxies of each correlated pair are at their respective cosmological distances from their redshifts. This becomes less accurate at smaller separations (e.g., with  $r_p$  less than a few Mpc), where the redshift difference of the pair of galaxies has a large contribution from the relative peculiar velocities and we tend to miss some correlated pairs. On the other hand, while their method would not miss such pairs, it over-counts the number of pairs with large projected separations. In practice, given the large value of  $\pi_{\max}$ , the fraction of either under-counted or over-counted pairs is tiny and such a subtle difference has no noticeable effect on the measurements.

The estimator we introduced makes a maximal use of the galaxy sample to achieve effectively volume-limited 2PCF measurements that have higher signal-to-noise ratio than those from the corresponding volume-limited sample. As discussed in the text, the method is mostly effective for faint galaxy samples in the power-law part of the luminosity function, as the number density of galaxies drops slowly towards high luminosity. For luminous galaxies, the rapid (exponential) decrease of the luminosity function towards high luminosity end makes the gain in volume from more luminous galaxies less important, as their contribution to the 2PCF is already small in the first place.